Thermotropic and structural effects of poly(malic acid) on fully hydrated multilamellar DPPC-water systems

Szilvia Berényi[a*], *Judith Mihály*[a], *Sándor Kristyán*[a], *Lívia Naszályi Nagy*[a], *Judit Telegdi*[b], *and Attila Bóta*[a]

Research Center for Natural Sciences, Hungarian Academy of Sciences,

[a]Institute of Molecular Pharmacology, Dept. of Biological Nanochemistry

[b]Institute of Materials and Environmental Chemistry, Dept. of Interfaces and Surface Modification

1025 Budapest, Pusztaszeri út 59-67, Hungary

* berenyi.szilvia@ttk.mta.hu

Abstract

The thermotropic and structural effects of low molecular weight poly(malic acid) (PMLA) on fully hydrated multilamellar dipalmitoylphosphatidylcholine (DPPC)-water systems were investigated using differential scanning calorimetry (DSC), small-angle X-ray scattering (SAXS), and freeze-fracture transmission electron microscopy (FFTEM). Systems of 20 wt% DPPC concentration and 1 and 5 wt% PMLA to lipid ratios were studied. The PMLA derivatives changed the thermal behavior of DPPC significantly and caused a drastic loss in

correlation between lamellae in the three characteristic thermotropic states (i.e., in the gel, rippled gel and liquid crystalline phases). In the presence of PBS or NaCl, the perturbation was more moderate. The structural behavior on the atomic level was revealed by FTIR spectroscopy. The molecular interactions between DPPC and PMLA were simulated via modeling its measured infrared spectra, and their peculiar spectral features were interpreted. Through this interpretation, the poly(malic acid) is inferred to attach to the headgroups of the phospholipids through hydrogen bonds between the free hydroxil groups of PMLA and the phosphodiester groups of DPPC.

Keywords: poly(malic-acid); DPPC; SAXS; FTIR; DSC; model membrane.

1. Introduction

Developing drug delivery systems that minimize harmful side-effects and increase both the drug bioavailability and the fraction of the drug accumulated in the required zone is a significant challenge for scientists. Polymeric nanoparticles opened new and innovative directions in the field of targeted drug delivery in recent decades. The multiple possible modifications of these nanoparticles enables various, drug molecules and targeting agents, to be dissolved, encapsulated, or attached to them. For drug delivery applications, nanoparticles must be biodegradable and the degradation products must not be toxic [1-6]. Poly(malic acid) (PMLA)-based nanoparticles (such as polycefin) are promising drug carrier candidates [1, 2, 6-11]. PMLA (Fig. 1) is a biocompatible polyester. PMLA is degradable by hydrolysis, leading to the production of nontoxic malic acid. The main chain of PMLA contains additional carboxylic groups, which can be used to introduce various bioactive ligands. Since

the first chemical synthesis of PMLA at the end of 1970s [12], many routes have been reported on the synthesis of racemic PMLA and the optically active poly(β-malic acid) [13].

The toxicity of polymer nanoparticles was studied from several aspects according to the literature. As reported by Maassen et al. [14], the cytotoxicity of nanospheres may be due to many factors, including (1) the release of degradation products, (2) the stimulation of cells and the subsequent release of inflammatory mediators, and (3) membrane adhesion [14, 15]. Martinez Barbosa et al. investigated not only the cytotoxicity of PMLA-based nanoparticles but also the toxicity of the degradation products [7]. They found relation between the cytotoxicity and the rate of polymer degradation. This relation may originate from the low molecular weight degradation products, which can easily diffuse into cells.

The goal of this study is to model the degradation products of low molecular weight PMLA and to investigate their effect on dipalmitoylphosphatidylcholine vesicles to obtain detailed information about the interactions between macromolecules and phospholipid bilayers. Apart from the fact that liposomes are widely used as vehicles for different drugs, they are often examined as model cell membranes because they contain lipid bilayers as the basic structural unit [16]. Differential scanning calorimetry (DSC), small-angle X-ray scattering (SAXS) and freeze-fracture transmission electron microscopy (FFTEM) are some prevalent methods to characterize liposomes and monitor the structural changes caused by other molecules. Thermal characterization with DSC provides information on the phase behavior of the phospholipid bilayers, as one can deduce the lamellarity from a SAXS pattern of a liposomal system and establish the characteristic distances between lamellae. FFTEM provides direct information about the morphology of the samples [17-19]. Infrared spectroscopy (IR) is used to study the structure and organization of lipid bilayers. Changes in the frequencies and widths of vibrational bands and/or splitting the spectral features provide information on the interactions between lipids and macromolecules [20, 21]. The vibrational spectra and

conformations of DPPC/PMLA and DPPC/water systems were modeled using *ab initio* and molecular mechanics [22-23] to understand the molecular interactions and motions involved. Although there is a vast amount of literature on the structural and vibrational behavior of very different DPPC systems using either experimental techniques or molecular mechanics and dynamics modeling, the literature on simulating the vibrational spectra of these systems, especially those investigated in this work, is very limited [24-26].

2. Materials and methods

2.1. Materials

Highly purified synthetic 1,2-dipalmitoyl-sn-glycero-3-phosphocholine (DPPC) was purchased from the NOF Corporation. Phosphate buffered saline (PBS) powder was obtained from Sigma-Aldrich. All materials were used without further purification.

The synthesis of the PMLA was based on the polycondensation reaction described by Kajiyama et al. [27-28], though an organic tin catalyst was not used. The polymeric substance was characterized by the IR spectrum, the specific rotation (α = -24.60; c = 2, water) and the degradation temperature (T = 207-209 °C). The molecular weight distribution of poly(malic acid) dissolved in water was surveyed by liquid chromatography-mass spectrometry. The solution contained molecules from monomers up to units consisting thirteen monomers; however, tetramers were the most common formations.

DPPC was hydrated in water to obtain a control sample with 20 wt% lipid content. Mixtures of PMLA and DPPC were prepared at 0.01 and 0.05 polymer/lipid weight ratios. PMLA was dissolved in water, and the solution was added to DPPC. The final lipid content was 20 wt%. Another batch of samples was prepared in 10 mM PBS solution (pH 7.4) instead of pure water. In every case, hydration was followed by heating to 60 °C, cooling to 4 °C, and reheating to 60 °C, while intensive vortexing was applied. The latter procedure was repeated several times to achieve homogeneous dispersions. Descriptions of the samples are presented in Table 1.

2.2. Differential scanning calorimetry

Samples were examined with a Setaram μDSC3 evo apparatus. All samples were scanned at least three times from 25 °C to 70 °C. The scan rate was initially 1 °C/min, 0.5 °C/min during the heating period, and 1 °C/min during the cooling period. An empty sample holder was used as a reference. The quantities of the samples used for the DSC measurements were approximately 10 mg.

2.3. Small-angle X-ray scattering

Small-angle X-ray scattering measurements were performed using a modified compact Kratky-type camera with slit collimation, and the intensity curves of SAXS were corrected by considering the geometry of the beam profile. Desmearing was performed using the software package “3Dview” that uses the direct desmearing method described by Singh et al. [29]. The X-ray source was a Cu-anode sealed X-ray tube. The scattering of Ni-filtered CuKα radiation (λ=1.542 Å) was recorded in the small-angle range from $s = 10^{-3}$ to 10^{-1} $Å^{-1}$. The scattering

variable is defined as $s=2\sin\Theta/\lambda$, where 2Θ is the scattering angle with the relationship $s=1/d$, where d is a characteristic periodicity in the sample. Thin-walled quartz capillaries with an average diameter of 1 mm were filled with the samples. The capillary containing the sample under study was inserted into a metal capillary holder, which was then placed into an aluminum block. To perform the measurements, this block was positioned directly in the beam line, and it was used as a thermal mass for controlled annealing at different temperatures. X-ray measurements were performed after 15 min of temperature stabilization of the samples at the respective temperatures. The exposure time was 1000 s for the X-ray detection.

2.4. Freeze-fracture transmission electron microscopy

Freeze-fracture electron microscopy was used for direct visualization of the evolved structures. The gold sample holders used in freeze-fracture were first incubated at 24 °C, i.e., the same temperature as the samples. Droplets of 1-2 μl of the sample were pipetted onto the gold sample holders and frozen by plunging the holders immediately into partially solidified freon for 20 seconds and stored in liquid nitrogen. Fracturing was performed at -100 °C with a Balzers freeze-fracture device (Balzers BAF 400D, Balzers AG, Vaduz, Liechtenstein). The replicas of the fractured faces etched at -100 °C were made by platinum-carbon shadowing, cleaned with a water solution of surfactant and washed with distilled water. The replicas were placed on 200-mesh copper grids and examined with a MORGANI 268D transmission electron microscope.

2.5. ATR-FTIR spectroscopy

ATR-FTIR (Attenuated Total Reflection Fourier Transform Infrared) measurements were recorded on a Varian 2000 FTIR (Scimitar Series) spectrometer with a 'GoldenGate' (Specac) ATR accessory (diamond ATR element, single reflection, 600 x 600 μm active area) using 256 scans at a resolution of 2 cm^{-1}. The spectral deconvolution of selected bands was performed using mixed Gaussian and Lorentzian functions. The GRAMS/32 software package was used for all spectral analyses.

2.6. Computer modeling

In the computer simulation, the Spartan [22] and Gaussian [23] packages were used for *ab initio* and density functional (DFT) calculations, as well as molecular mechanics (MM) calculations, to estimate equilibrium geometries, energies, thermodynamic properties and frequencies (to model infrared spectra). We introduce a goal-oriented calculation in the discussion.

3. Results and discussion

3.1. DSC experiments

DPPC lipids spontaneously form multilamellar vesicles (MLVs) in water. The fully hydrated DPPC/water system undergoes two phase transitions with increasing temperature in the temperature range examined: a pretransition from the gel state ($L_{\beta'}$) to the rippled gel state ($P_{\beta'}$) at approximately 34 °C, and a main transition to the liquid crystalline state (L_{α}) at 41 °C. The pretransition exhibits a relatively small enthalpy change, which is mainly due to the

rotation of the polar headgroups. The main transition is due to the cooperative melting of the hydrocarbon chains, wherein certain C-C single bond configurations change from *trans* to *gauche*. The main transition exhibits a well-defined transition temperature (41.1 °C) and enthalpy change (ΔH = 36.5 kJ/mol) [30]. These phase transitions can also be followed in the presence of foreign molecules by DSC (Fig. 2) . The thermograms are very sensitive to changes, e.g., when DPPC is suspended in 10 mM PBS solution instead of ion-exchanged water, where the peak of the main transition becomes sharper and more symmetric. The shape of the peak refers to the cooperativity of the chain melting, i.e., a sharper peak indicates that more molecules are simultaneously melting. [18, 31-32]

Thermograms of hydrated DPPC/PMLA systems are presented in Fig. 2, and the phase transition parameters are listed in Table 2. Even an amount of PMLA as small as 1 wt% added to the lipid (PCPMw01) affects the thermal behavior of the liposomes. The effect becomes noticeably heterogeneous according to the two shoulders of the main transition peak (43.1 °C and 43.9 °C). A shift of the pretransition peak to a lower temperature is observed. The ΔH of the pretransition and main transition decreases in the presence of PMLA. In addition, there is a decrease in the value of the cooperative unit of the main transition, which indicates a destabilization of the membrane [33]. Due to the observed decrease in the temperature and the enthalpy change of the pretransition peak, the PMLA is likely adsorbed to the headgroup-region of the bilayers. This thermal behavior can be due to the altered charge state of the phosphocholine-group (i.e., the PMLA at this concentration produces pH 2.2 and the pK_a of DPPC is 3.8-4.0 [34], so under these conditions DPPC is positively charged) and/or due to the adsorption of the PMLA onto the surface. Because the peripheral association of molecules to the surface of the bilayers can lead to high temperature shoulders [35], we expect the latter.

The sample containing a larger amount of polymer (PCPMw05) exhibits an obviously perturbed endotherm. The temperature of the pretransition peak does not change, though ΔH

decreases, indicating an increased mobility in the polar region. The main transition exhibits a complex peak, containing a shoulder at 43.0 °C and a hump at approximately 45 °C. In addition, a new, less intensive peak evolves at 48.1 °C. These changes observed in the DSC endotherm suggest that PMLA binds to the bilayer surface and that this interaction becomes stronger with increasing polymer concentration. It is difficult to simply determine from the DSC measurements whether the forces between poly(malic acid) and DPPC arise from charge-charge interactions between carboxylate anions and phosphocholine groups or from hydrogen bonding between free –OH groups and the phosphodiester headgroup [36].

According to the DSC measurements (Fig. 2), when 10 mM PBS solution was used for hydration instead of pure water, liposomes were less perturbed when 1 wt% PMLA was added (PCPMb01). Neither the position nor the enthalpy change of the pretransition peak altered significantly compared to the DPPC/PBS system; only the peak of the main transition shifted slightly to higher temperature, and the corresponding ΔH increased. This indicates a type of stabilization of the gel phase [37]. There is also a significant decrease in the cooperativity due to the presence of the polymer; however, the rate of this change is less than that observed for PCPMw01. It seems that the effect of PMLA is not predominant in PBS because of the presence of NaCl and/or because of the neutral pH.

The thermograms were significantly changed when 5 wt% PMLA was added to the lipids (PCPMb05). The pretransition peak shifted to a higher temperature, and ΔH decreased appreciably. A complex peak appeared that was related to the split of the main transition into two distinct ones (42.1 °C and 43.1 °C) with a broad shoulder at approximately 44.6 °C. Furthermore, a small peak was observed at 48.0 °C, which is similar to the case of PCPMw05. It seems that phosphate buffered saline solution does not influence the strong interaction between the lipid bilayer surface and PMLA when the polymer is added at 5 wt% to the lipids. Presumably, when less poly(malic acid) is present, the sodium ions screen the charges

of PMLA as well those of the lipids, thereby explaining why the thermotropic character of the bilayers does not change so drastically.

3.2. SAXS measurements

Multilamellar liposomes contain many periodically packed bilayers with an average periodicity that ranges between 50-70 Å, which can be measured by small-angle X-ray scattering. Bragg peaks appear in the SAXS pattern at the position s = n/d, where n is the order of the reflection. The fully hydrated DPPC/water system exhibits a well-established structure. The characteristic distances of the layer arrangement are as follows: 63 Å in $L_{\beta'}$ phase, 71 Å in $P_{\beta'}$ phase and 65 Å in L_{α} phase. In accordance with the thermotropic behavior of these systems, structural studies were performed at 25 °C, 38 °C, and 46 °C (Fig. 3, Table 3). Our results are in agreement with the literature data [38]. Furthermore, the shape of a reflection peak in a SAXS curve provides structural information. A sharper peak indicates that the stacks of layers are more ordered. Even the presence of as little as 10 mM of PBS solution causes a little broadening of the peaks, especially for the $P_{\beta'}$ phase, but it does not influence the size of the periodic distances.

The addition of PMLA causes a major perturbation in the structure of the vesicles. The relevant SAXS patterns are presented in Fig. 3. The major change in the patterns of the DPPC/PMLA/water systems is that no Bragg-reflections appear, and only a broad “hump” is observed. This hump corresponds to the form factor of single layers F(s) (the Fourier transform of the electron density profile), the appearance of which indicates that the correlation between the layers in the emulsion is very weak [39-42].

These observations stated above indicate that PMLA disrupts the regular multilamellar arrangement of the liposomes. This disruption may be due to the hydrolysis of lipids caused by the low pH or to the steric and/or electrostatic effect of the polymer when it is attached to the headgroups, causing the layers to swell. To determine the origin of this phenomenon, NaCl was added to the sample PCPMw01 and subsequently vortexed intensively, followed by characterization using SAXS. Fig. 3 reveals that Bragg-peaks reappear (s_1=1/65 Å) in the SAXS measurement, but they are broadened in comparison to the pure system. Additionally, the characteristic distances of the layer arrangement increase in the gel state but decrease in rippled-gel and liquid crystalline phases compared to both the DPPC/H_2O and DPPC/PBS systems. This change in the characteristic distances indicates that the multilamellar structure is partially reconstructed and that PMLA is located between the lipid bilayers. It seems that chemical deconstruction of lipids did not occur at a considerable rate; otherwise, the layer packing would not have been reconstructed. We also investigated the effect of low pH on the vesicles by adding dilute hydrochloric acid solution (with pH 2.2, i.e., the same pH as that of the PMLA solution previously used) to DPPC. The results (not published) indicate that due to the low pH, the layers started to swell. The swelling can be understood as follows. At this low pH, lipids are positively charged (as mentioned above), and electrostatic repulsion thus occurs between the layers.

We assume that the significant perturbation caused by PMLA on the structure of DPPC/water vesicles is due to the alteration in the electric charges on the lipid headgroups. When these charges are screened, multilamellar liposomes can form that heterogeneously contain PMLA between the bilayers.

For the samples that were prepared in buffer solution, SAXS patterns (presented in Fig. 3) also indicate that the presence of PMLA causes minor changes in the characteristics of the layer arrangement. At a 0.01 polymer/lipid weight ratio, the Bragg-peaks are broadened,

which indicates the presence of the polymer. The characteristic distance increases significantly only in the liquid crystalline phase. The broadening of the Bragg-peaks in the $L_{\beta'}$ and $P_{\beta'}$ phases becomes more significant at a 0.05 weight ratio. Furthermore, the distances between layers increase in all three phases. We can thus conclude that PMLA is positioned between the bilayers and causes a loss of correlation between their arrangements.

3.3. FFTEM observations

TEM images obtained on replicas from freeze-fractured samples provide visual information on the effect of PMLA on DPPC-based vesicles. Fig. 4/B shows that there are no arranged layers in the PMPCw05 sample : loosely packed stacks of curved layers are present, while the water regions between them are extremely extended, so the correlation of the layers is hindered, causing the disappearance of the Bragg reflections in the SAXS patterns (Fig. 3). In contrast, multiple well-correlated layers are present in the PMPCb05 sample (Fig 4/C): large, laterally micrometer-size, tightly packed layers are visible, resulting in the reconstructed Bragg peaks shown in Fig. 3.

3.4. FTIR spectroscopy

To obtain information on the possible interactions between PMLA and lipid molecules, infrared spectra of hydrated DPPC/PMLA systems were measured at room temperature. The spectral regions selected for investigation were the symmetric CH_2 stretching vibration (2588-2580 cm^{-1}), the carbonyl stretching mode C=O (1800-1680 cm^{-1}) and the phosphate headgroup vibration region (1260-1000 cm^{-1}) (Fig. 5). No significant spectral differences were observed due to the presence of PMLA in the DPPC system compared to the control

DPPC/water suspension. This lack of difference indicates that, despite the high acidity of the poly(malic acid) solution (pH=2.2), prompt destructive hydrolysis of the phospholipid molecules does not occur.

3.4.1. *Lipid order and packing*

The frequency of the peak position of the methylene stretching band (ν_s CH_2) is a common parameter used to detect the conformational disorder and mobility of the hydrocarbon chain [21]. No notable change was observed in the ν_s CH_2 frequency (Fig. 5) due to the presence of PMLA in the DPPC system, indicating that poly(malic acid) has no effect on the lipid order and packing under our experimental conditions.

3.4.2. *Sites of hydrations*

The phosphate and carbonyl frequencies are widely used as sensors for changes in hydration at the interface region or at the headgroup. The polar-apolar interface of DPPC is represented by ester carbonyl groups with a C=O stretching band between 1800 and 1600 cm^{-1}. In highly hydrated bilayers, this band splits into two overlapping components: a high wavenumber band at approximately 1742 cm^{-1} of the non-hydrogen bonded C=O groups and a low wavenumber band at approximately 1728 cm^{-1}, due to the hydrogen bonding of the C=O groups [43-46]. The exact positions of these bands are also affected by the geometry of the glycerol moieties and the packing of the alkyl chains. Fig. 6 presents the results of a curve fitting analysis (band positions were estimated using the second derivative, and band shapes were approximated by mixed Gaussian and Lorentzian functions until the minimal χ^2 parameter was obtained). For the DPPC/PMLA/water system with rather high acidity, the

relative intensity of the non-hydrogen bonded C=O band increases compared to that of the "pure" DPPC/water liposomes (Fig. 6), indicating a dehydration of the lipid interface region. In the presence of the buffer, however, this phenomenon is suppressed. Assuming that no change in the alkyl region occurs, the variation in the overall band shape of the C=O band can be related to the change in the "secondary hydration shell" of the lipid. This altered secondary hydration shell can contribute to the variations of the dipole potential of the lipid membrane surface.

The phosphate moiety of the headgroup also has characteristic vibrations in the DPPC spectrum [47-48]. Asymmetric and symmetric stretching modes of the PO_2^- group exhibit bands in the region from 1230-1220 cm^{-1} and at 1085 cm^{-1}, respectively, with the former being superimposed onto the weak band series of the CH_2 wagging progression [49]. The R-O-P-O-R' stretching of phosphate-diester appears as a shoulder near the ν_s PO_2^- band at approximately 1060 cm^{-1}. The asymmetric PO_2^- stretching (ν_{as} PO_2^-) band is the most sensitive for the hydrated state: due to the H-bonded water molecules, it exhibits the maximum at 1222 cm^{-1} in the fully hydrated state, while it shifts towards higher wavenumbers (~1243 cm^{-1}) in the dry state. In contrast to the dehydration experienced for the C=O groups, different concentrations of PMLA in liposomes does not change the position of ν_{as} PO_2^-. Only the relative intensities of the ν_s PO_2^- and ν R-O-P-O-R' bands changed slightly in the spectra of the DPPC/PMLA system compared to the case of the "pure" DPPC/water system, due to the presence of foreign molecules between the lipid bilayers (Fig. 5).

Investigating the ν_{as} PO_2^- stretching mode in the DPPC/PMLA dry film spectra, the H-bonded PO_2^- asymmetric stretching band of the phosphate moiety is still present (at 1222 cm^{-1}), and its intensity increases with increasing concentration of PMLA (Fig. 7). This observed behavior demonstrates a direct interaction between DPPC and PMLA molecules. One can presume that the occurring free OH groups of malic acid/poly(malic acid) might

mimic the water of hydration. Due to steric hindrance, the carbonyl groups of DPPC positioned at the interface region are not accessed by PMLA.

3.4.3. *Computer simulation of the molecular interactions in the DPPC/PMLA system via modeling its measured infrared spectra*

We have considered an individual DPPC from the bilayer, four water molecules, and a malic acid monomer in calculating the IR spectra. The notations DPPC (dehydrated), DPPC/water and DPPC/malic acid/water refer to the experimentally prepared systems as described above, while the notations DPPC, DPPC+4H_2O and DPPC+malic acid refer to our computing models. The equilibrium structures are shown in Fig. 8. The direction of the dipole moment exhibits almost no change, indicating that the global structure of a bilayer does not change noticeably with respect to this calculated value.

The Spartan program (molecular mechanics) was used to calculate the absorption frequencies of the IR spectra, focusing on the PO_2^- functional group in DPPC. This group yields characteristic bands, and the different molecular environments (Fig. 8) produce different effects on the peaks. The plot of calculated PO_2^- vibrations is shown in Fig. 9. Differences between the three systems are observed in the spectral region over 1250 cm^{-1}: experimental PO_2^- vibrations of hydrated/dehydrated DPPC were obtained at 1222/1243 cm^{-1} (21 cm^{-1} shift, Fig. 7), which are comparable to our calculated values 1263/1287 (24 cm^{-1} shift, Fig. 9). We conclude from our computer investigation that the partially positive hydrogen atoms in water molecules quench the vibration of PO_2^- via the negative electron lobes of oxygen atoms in PO_2^-, which is plausible.

After drying the DPPC/malic acid/water system to form the DPPC/malic acid system, the dehydrated PO_2^- vibration interestingly appears at approximately the same position as the

hydrated PO_2^- (1222 cm^{-1}, Fig. 7), while this peak appears at 1243 cm^{-1} for a normal water-free DPPC system (Fig. 7). The malic acid can substitute for the effect of water in this respect, i.e., according to Fig. 8, certain hydrogen atoms in malic acid play a similar role as the hydrogen atoms in water molecules when quenching the PO_2^- vibration. The calculation (Fig. 9) is remarkable because the DPPC system (dehydrated, PO_2^- peak at 1287 cm^{-1}) separates from the DPPC+4H_2O (hydrated, PO_2^- peak at 1263 cm^{-1}) and DPPC+malic acid (PO_2^- peak at 1269 cm^{-1}) system with approximately the same frequency shift. We conclude from our computer investigation that the electron lobes of oxygen atoms in the PO_2^- group in DPPC and the hydrogen atoms of two OH groups and the hydrogen atom of CH in the malic acid inter-molecularly affect each other in the same manner as the hydrogen atoms in water in the DPPC+4H_2O system, which is also plausible.

4. Conclusion

The results of this study indicate that poly(malic acid) interacts with the headgroups of phospholipids and changes the thermal properties and packing feature of the DPPC bilayers. From the DSC endotherms, the ΔH of the pretransition and main transition decreases, and a reduction in the cooperativity of the main transition is observed when PMLA is present, compared to the case of a pure DPPC/water system. Meanwhile, SAXS results suggest that PMLA hinders DPPC to form a multilamellar structure, consisting of primarily miscorrelated layers. This multilamellar structure can be attributed to the low pH caused by the polyacid and thus to the change in the electrostatic state of the lipids.

Using PBS buffer instead of pure water makes the perturbation caused by PMLA less drastic. According to the DSC endotherms, when the polymer/lipid ratio is 1 wt%, only the

reduced cooperativity indicates the presence of PMLA. A complex endotherm is observed at 5 wt% PMLA, caused by a strong interaction between the layer surface and polymer. Due to the buffer effect, MLVs can be formed, as indicated by SAXS measurements and electron micrographs; however, the layers are less correlated and the characteristic distances increase due to the presence of the incorporated polymer.

FTIR spectroscopy demonstrates that there is a change in the dipole potential of the lipid membrane surface when PMLA is present compared to the case of the DPPC/water system. However, this change is suppressed in the presence of PBS. In addition, hydrogen bonds are demonstrated to form between the free hydroxil groups of PMLA and the phosphodiester groups of DPPC. The incorporation of the polymer results in a reduced hydration in the polar region and may decrease the dipole potential in the lipid membrane interface because of the contribution of water molecules. Eventually, the changes in the dipole potential may increase the thickness of the water layer at each side of bilayers, where the significant loss in layer correlation exists, as observed directly from the SAXS patterns.

In summary, the low molecular weight PMLA interacts with the headgroups of lipids in liposomes and causes the swelling of the layers in the absence of buffer. However, when the acidity of the polymer is not dominant, PMLA does not significantly disrupt the structure of liposomes. Thus, low molecular weight PMLA likely does not disrupt cell membranes either.

These results can impact the field of liposomal drug delivery, as attaching charged polymers (such as PMLA) to the surface of unilamellar liposomes can provide them with steric stability.

Acknowledgments.

The authors thank Teréz Kiss for the FFTEM investigations, Pál Szabó for performing the LC-MS experiments, and András Wacha and Zoltán Varga for the helpful discussions. This work was supported by the National Innovation Office (NIH, Hungary) under grant agreements NKFP_07-A2-2008-0247 and CNK-81056.

References:

[1] E. Segal, R. Satchi-Fainaro, Design and development of polymer conjugates as anti-angiogenic agents, Adv. Drug. Deliv. Rev. 61 (2009) 1159-1176.

[2] T. Wang, J.R. Upponi, V.P. Torchillin, Design of multifunctional non-viral gene vectors to overcome physiological barriers: Dilemmas and strategies, Int. J. Pharm. 427 (2012) 3-20.

[3] K.S. Soppimath, T.M. Aminabhavi, A.R. Kulkarni, W.E. Rudzinski, Biodegradable polymeric nanoparticles as drug delivery devices, J. Cont. Rel. 70 (2001) 1-20.

[4] J.M. Chan, P.M. Valencia, L. Zhang, R. Langer, O.C. Farokhzad, Polymeric Nanoparticles for drug delivery, Method Mol. Biol. 624 (2010) 163-175.

[5] M.L. Hans, A.M. Lowman, Biodegradable nanoparticles for drug delivery and targeting, Curr. Opin. Solid St. M. 6 (2002) 319-327.

[6] S. Stolnik, L. Illum, S.S. Davis, Long circulating microparticulate drug carriers, Adv. Drug. Deliv. Rev. 16 (1995) 195-214.

[7] M.E. Martinez Barbosa, S. Cammas, M. Appel, G. Ponchel, Investigation of the degradation mechanisms of poly(malic acid) esters in vitro and their related cytotoxicities on J774 macrophages, Biomacromolecules 5 (2004) 137-143.

[8] S. General, A.F. Thünemann, pH-sensitive nanoparticles of poly(amino acid) dodecanoate complexes, Int. J. Pharm. 230 (2011) 11-24.

[9] J.Y. Ljubimova, M.Fujita, A.V. Ljubimov, V.P. Torchilin, K.L. Black, E. Holler, Poly(malic acid) nanoconjugates containing various antibodies and oligonucleotides for multitargeting drug delivery, Nanomedicine (London) 3 (2008) 247-265.

[10] J.Y. Ljubimova, M. Fujita, N.M. Khazenzon, B.S. Lee, S. Wachsmann-Hogiu, D.L. Farkas, K.L. Black, E. Holler, Nanoconjugate based on polymalic acid for tumor targeting, Chem-Biol. Interact. 171 (2008) 195-203.

[11] Z. W. Huang, V. Laurent, G. Chetouani, J.Y. Ljubimova, E. Holler, T. Benvegnu, P. Loyer, S. Cammas-Marion, New functional degradable and bio-compatible nanoparticles based on poly(malic acid) derivatives for site-specific anti-cancer drug delivery, Int. J. Pharm. 423 (2012) 84-92.

[12] M. Vert, R. W. Lenz, Preparation and properties of poly-beta-malic acid: A functional polyester of potential biomedical importance, ACS Polym. Preprints 20 (1979) 608-611.

[13] M. Vert, Chemical routes to poly(β-malic acid) and potential applications of this water-soluble bioresorbable poly(β-hydroxy alkanoate), Polym. Degrad. Stab., 59 (1998) 169-175.

[14] S. Maassen, E. Fattal, R. Muller, P. Couvreur, Cell cultures for the assessment of toxicity and uptake of polymeric drug carriers, S.T.P. Pharma Sci. 3 (1993) 11-22.

[15] C. Vauthier, C. Dubernet, E. Fattal, H. Pinto-Alphandary, P. Couvreur, Poly(alkylcyanoacrylates) as biodegradable materials for biomedical applications, Adv. Drug Del. Rev., 55 (2003) 519-548.

[16] C. Peetla, A. Stine, V. Labhasetwar, Biophysical Interactions with Model Lipid Membranes Applications in Drug Discovery and Drug Delivery, Mol. Pharm. 6 (2009) 1264-1276.

[17] Gregory Gregoriadis (Ed.), Liposome Technology Third Edition, Vol I, Informa Healthcare USA, Inc. 2007

[18] V.P. Torchilin, V. Weissig, Liposomes: A practical approach, Oxford University Press, 2003.

[19] M.M. Koerner, L.A. Palacio, J.W. Wright, K.S. Schweitzer, B.D. Ray, Electrodynamics of Lipid Membrane Interactions in the Presence of Zwitterionic Buffers, Biophys. J. 101 (2011) 362-369.

[20] R.N.A.H. Lewis, R.N. McElhaney, The structure and organization of phospholipid bilayers as revealed by infrared spectroscopy, Chem. Phys. Lipids 96 (1998) 9-21.

[21] Z.D. Schultz, I.W. Levin, Vibrational Spectroscopy of Biomolecules, Annu. Rev. Anal. Chem. 4 (2011) 343-366.

[22] W. J. Hehre, W. W. Huang, P. E. Klunzinger, B. J. Deppmeier, A. J. Driessen, Spartan Manual. Wavefunction, Inc., 18401Von Karman Ave., Suite 370, Irvine, CA 92612.

[23] M. J. Frisch, G. W. Trucks, H. B. Schlegel, G. E. Scuseria, M. A. Robb, J. R. Cheeseman, V. G. Zakrzewski, J. A. Montgomery, Jr., R. E. Stratmann, J. C. Burant, S. Dapprich, J. M. Millam, A. D. Daniels, K. N. Kudin, M. C. Strain, O. Farkas, J. Tomasi, V. Barone, M. Cossi, R. Cammi, B. Mennucci, C. Pomelli, C. Adamo, S. Clifford, J. Ochterski, G. A. Petersson, P. Y. Ayala, Q. Cui, K. Morokuma, D. K. Malick, A. D. Rabuck, K. Raghavachari, J. B. Foresman, J. Cioslowski, J. V. Ortiz, B. B. Stefanov, G. Liu, A. Liashenko, P. Piskorz, I. Komaromi, R. Gomperts, R. L. Martin, D. J. Fox, T. Keith, M. A. Al-Laham, C. Y. Peng, A. Nanayakkara, C. Gonzalez, M. Challacombe, P. M. W. Gill, B. Johnson, W. Chen, M. W. Wong, J. L. Andres, C. Gonzalez, M. Head-Gordon, E. S. Replogle, J. A. Pople, Gaussian 98, Revision A. 6; Gaussian, Inc.: Pittsburgh, PA, 1998.

[24] W. Pohle, C. Selle, H. Fritzsche, H. Binder, Fourier transform infrared spectroscopy as a probe for the study of the hydration of lipid self-assemblies. I. Methodology and general phenomena, Biospectroscopy 4 (1998) 267-280.

[25] D. L. Elmore, S. Shanmukh, R. A. Dluhy, A Study of Binary Phospholipid Mixtures at the Air-Water Interface Using Infrared Reflection-Absorption Spectroscopy and 2D IR $\beta\nu$ Correlation Analysis, J.Phys.Chem.A. 106 (2002) 3420-3428.

[26] H. Bensikaddour, K. Snoussi, L. Lins, F. Van Bambeke, P. M. Tulkens, R. Brasseur, E. Goormaghtigh, M.P. Mingeot-Leclercq, Interactions of ciprofloxacin with DPPC and DPPG: Fluorescence anisotropy, ATR-FTIR and 31P NMR spectroscopies and conformational analysis, Biochimica et Biophysica Acta 1778 (2008) 2535-2543.

[27] T. Kajiyama, T. Taguchi, H. Kobayashi, K. Kataoka, J. Tanaka, Synthesis of high molecular weight poly(α,β-malic acid) for biomedical use by direct polycondensation, Polym. Degrad. Stab. 81 (2003) 525-530.

[28] T. Kajiyama, H. Kobayashi, T. Taguchi, K. Kataoka, J. Tanaka, Improved Synthesis with High Yield and Increased Molecular Weight of Poly(α,β-malic acid) by Direct Polycondensation, Biomacromol. 5 (2004) 169-174.

[29] M.A. Singh, S.S. Gosh, R.F. Shannon Jr., A Direct Method of Beam-Height Correction in Small-Angle X-Ray Scattering, J. Appl. Cryst. 26 (1993) 787-794.

[30] C. Grabielle-Madelmont, R. Perron, Calorimetric studies on phospholipid–water systems. I: DL-dipalmitoylphosphatidylcholine(DPPC)–water system, J. Colloid Interf. Sci. 95 (1983) 471-482.

[31] M. Pantusa, R. Bartucci, L. Sportelli, Calorimetric and spin-label ESR studies of PEG:2000-DPPE containing DPPC/lyso-PPC mixtures, Colloid Polym. Sci., 285 (2007) 649-656.

[32] B.G. Auner, M.A.A. O'Neill, C. Valenta, J. Hadgraft, Interaction of phloretin and 6-ketocholestanol with DPPC-liposomes as phospholipid model membranes, Int, J. Pharm 294 (2005) 149-155.

[33] S. Banerjee, T.K. Pal, S.K. Guha, Probing molecular interactions of poly(styrene-co-maliec acid) with lipid matrix models to interpret the therapeutic potential of the co-polymer, Biochimica et Biophysica Acta 1818 (2012) 537-550.

[34] G. Cevc, Phospholipids Handbook, Taylor & Francis, 1993

[35] A. Blume, P. Garidel, Lipid model membranes and biomembranes. in: P.K. Gallagher, M.E. Brown (Eds.), The Handbook of Thermal Analysis and Calorimetry. From Macromolecules to Man. 1st ed. Elsevier, Amsterdam, 1999, pp 109–173.

[36] K. Seki, D.A. Tirrell, pH-Dependent Complexation of Poly(acrylic acid) Derivatives with Phospholipid Vesicle Membranes, Macromolecules 17 (1984) 1692-1698.

[37] J.C. Schwarz, H. Kahlig, N.B. Matsko, M. Kratzel, M. Husa, C. Valenta, Decrease of Liposomal Size and Retarding Effect on Fluconazole Skin Permeation by Lysine Derivatives, J. Pharm. Sci. 100 (2011) 2911-2919.

[38] B.G. Tenchov, H. Yao, I. Hatta, Time-resolved x-ray diffraction and calorimetric studies at low scan rates I. Fully hydrated dipalmitoylphosphatidylcholine (DPPC) and DPPC/water/ethanol phases, Biophys. J. 56 (1989) 757-768.

[39] R. Zhang, R. M. Suter, J.F. Nagle, Theory of the structure factor of lipid bilayers, Phys. Rev. E 50 (1994) 5047-5060.

[40] Guinier, A.: X-ray diffraction. San Francisco: Freeman, 1963.

[41] G. Pabst, R., Koschuch, B. Pozo-Navas, M. Rappolt, K. Lohner, P. Laggner, Structural analysis of weakly ordered membrane stacks. J. Appl. Cryst. 36 (2003)1378-1388.

[42] A. Bóta, Z. Varga, G. Goerigk, Vesicles as reactors of nanoparticles, J. Appl. Cryst. 40 (2007) 259-263.

[43] H.H. Mantsch, D. Chapman, Infrared Spectroscopy of Biomolecules, Wiley-Liss, New York, 1996.

[44] K. Cieslik-Boczula, J. Swed, A. Jaszczyszyn, K. Gasiorowski, A. Koll, Interactions of dihydrochloride fluphenazine with DPPC liposomes: ATR-IR and 31P NMR studies, J. Phys. Chem. B 113 (2009) 15495-15502.

[45] M. Manrique-Moreno, J. Howe, M. Suwalsky, P. Garidel, K. Brandemburg, Physicochemical interaction study of non-steroidal anti-inflammatory drugs with dimiristoylphosphatidylethanolamine liposomes, Letters in Drug Design & Discovery 7 (2010) 50-56.

[46] E.A.A.M. Vernooij, J.J. Kettenes-van den Bosch, D.J.A. Crommelin, Fourier transform infrared spectroscopic determination of the hydrolysis of poly(ethylene glycol)-phosphatidylethanolamine-containing liposomes, Langmuir 18 (2002) 3466-3470.

[47] J.L.R. Arrondo, F.M. Goni, J.M. Macarulla, Infrared spectroscopy of phosphatidylcholines in aqueous suspension A study of the phosphate group vibrations, Biochimica et Biophysica Acta 794 (1984) 165-168.

[48] W. Pohle, D.R. Gauger, H. Fritzsche, B. Rattay, C. Selle, H. Binder, H. Böhlig, FTIR-spectroscopic characterization of phosphocholine-headgroup model compounds, J. Mol. Struc, 563-564 (2001) 463-467.

[49] L. Senak, D. Moore, R. Mendelsohn, CH2 wagging progressions as IR probes of slightly disordered phospholipid acyl chain states, J. Phys. Chem. 96 (1992) 2749-2754.

Figures

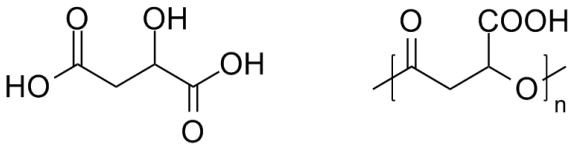

Figure 1. Malic acid and poly(malic acid).

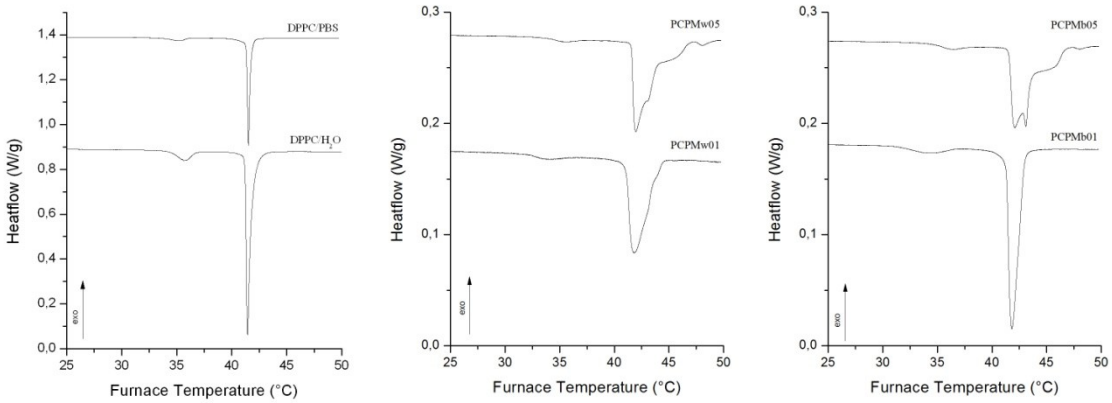

Figure 2. DSC thermograms of 20 wt% DPPC in double distilled water (DPPC/H_2O) and PBS solution (10 mM, pH 7.4); water-based systems: 1 wt% PMLA/DPPC ratio (PCPMw01) and 5 wt% PMLA/DPPC ratio (PCPMw05); phosphate buffered saline-based systems: 1 wt% PMLA/DPPC ratio (PCPMb01) and 5 wt% PMLA/DPPC ratio (PCPMb05).

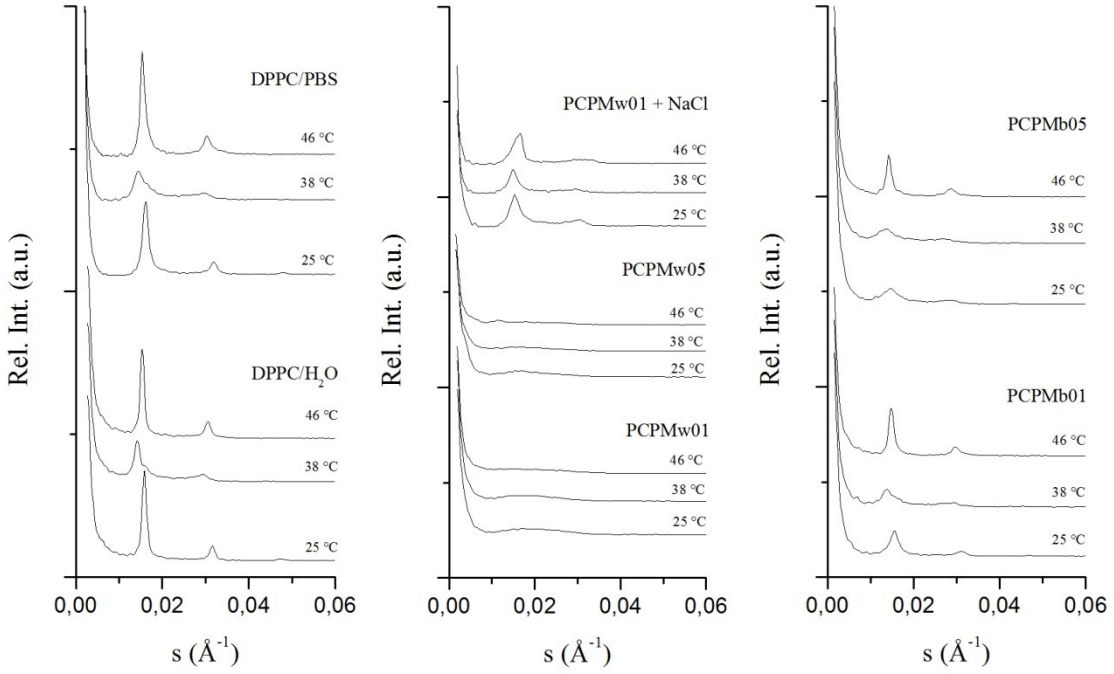

Figure 3. SAXS patterns of hydrated DPPC vesicles measured at different temperatures: PMLA-perturbed hydrated DPPC systems (PCPMw01, PCPMw05); PBS solution-hydrated vesicles (PCPMb01, PCPMb05).

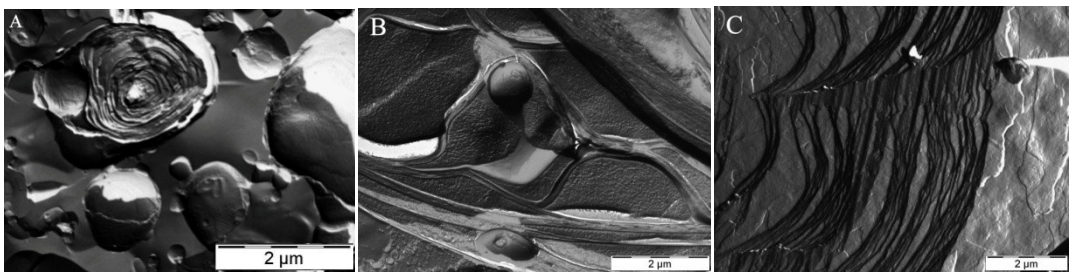

Figure 4. Freeze-fracture TEM images of samples DPPC/ H_2O (A), PCPMw05 (B) and PCPMb05 (C).

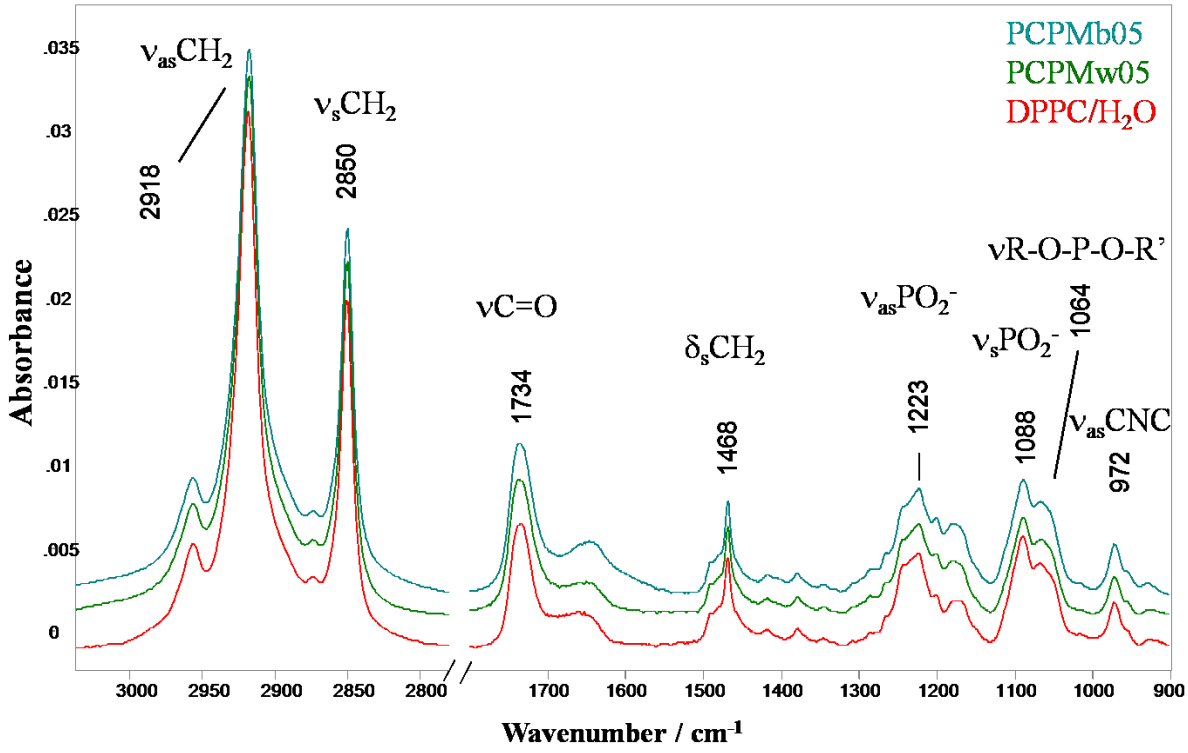

Figure 5. ATR-FTIR spectra of liposomes recorded at room temperature (24 °C). From bottom to top: DPPC/water; DPPC/PMLA/H_2O system (PCPMw05); DPPC/PMLA/PBS system (PCPMb05).

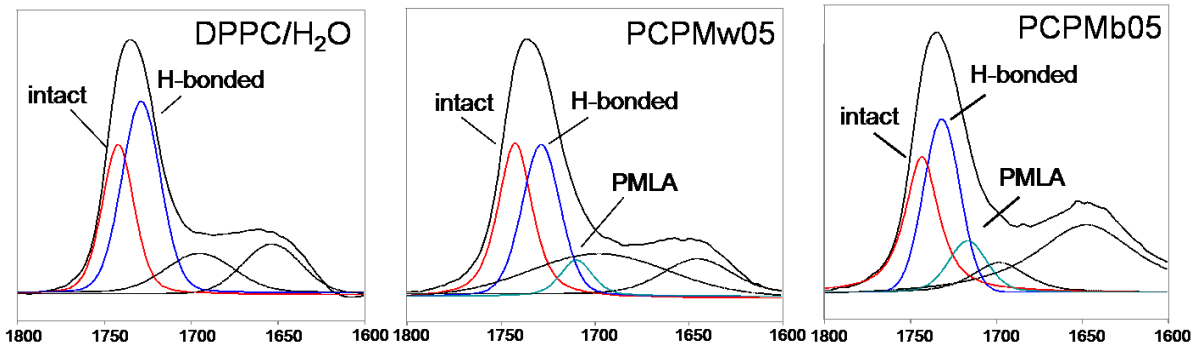

Figure 6. ATR-FTIR spectra of the carbonyl stretch region (1800-1600 cm^{-1}). The solid black lines are the measured spectra; the red and the blue lines are the fitted bands corresponding to intact and H-bonded C=O groups, respectively; the green lines are fitted bands belonging to the C=O stretch of the malic acid/poly(malic acid) components; and the dashed lines are fitted bands, which may be related to fatty acids (impurities or hydrolysis results) and residual water (inaccurate spectral subtraction).

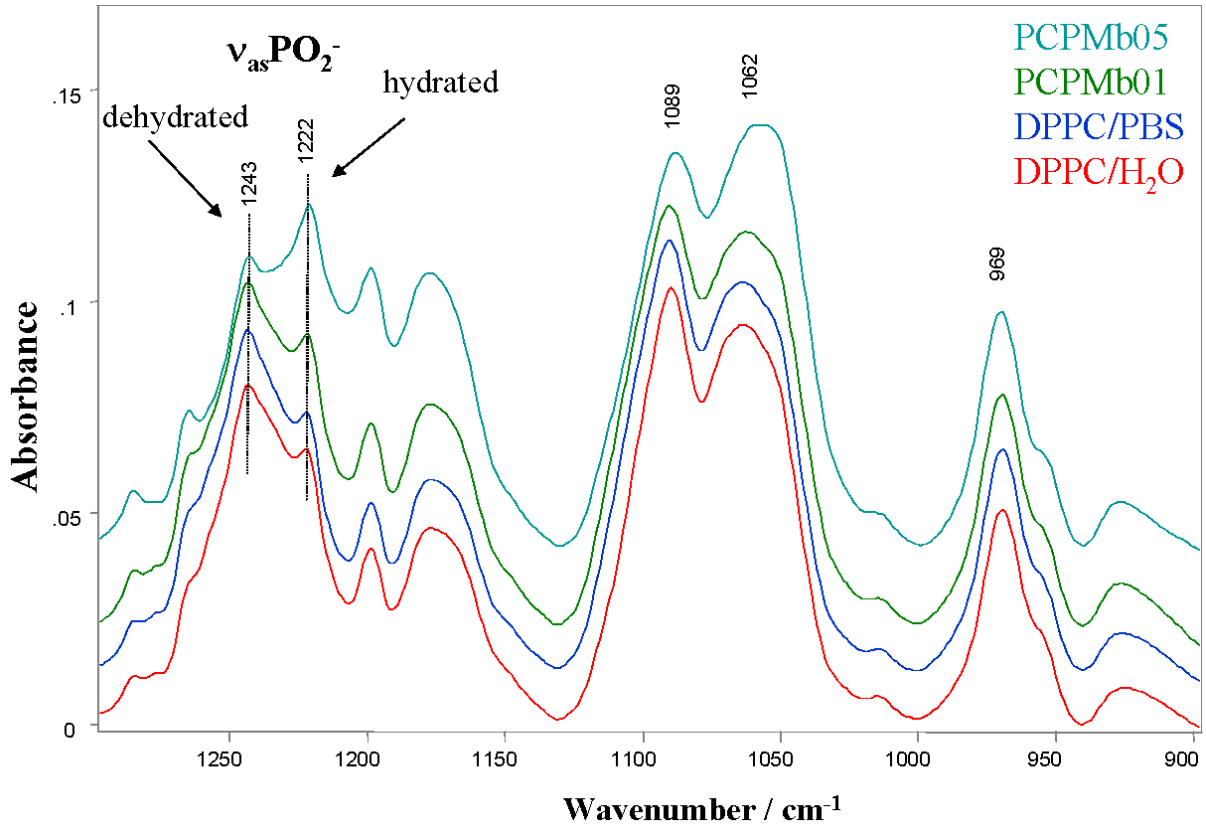

Figure 7. ATR-FTIR spectra of dry films of PMA/ DPPC/PBS systems. For comparison, dry film spectra of pure DPPC/water and DPPC/PBS are presented. From bottom to top: DPPC/water system; DPPC/PBS system; DPPC/PMLA/PBS systems with 1 wt% PMLA/DPPC ratio (PCPMb01) and 5 wt% PMLA/DPPC ratio (PCPMb05).

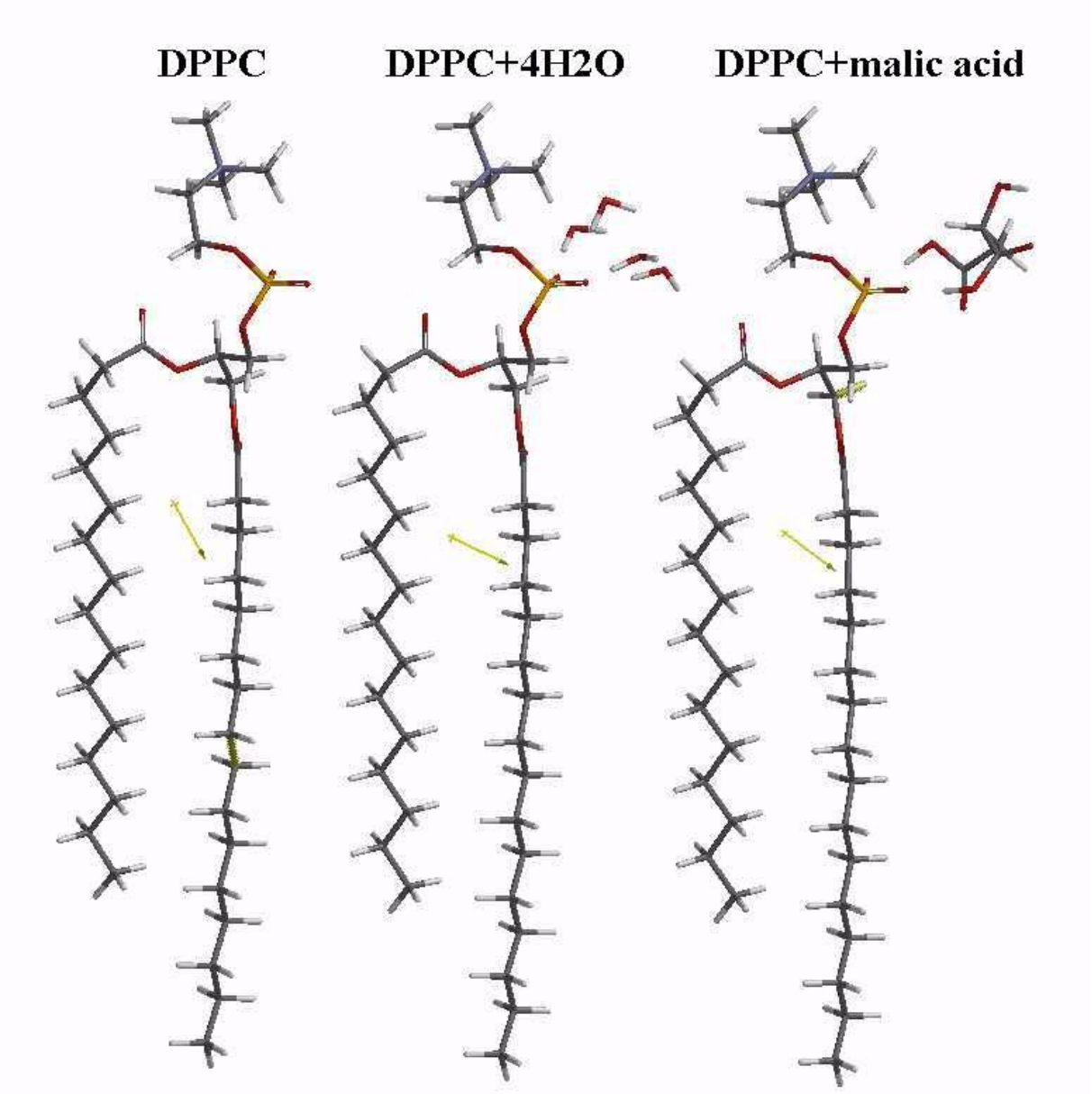

Figure 8. Different simulated molecular environment for the headgroup of DPPC from a bilayer: without guest molecules, in contact with four water molecules, and with malic acid.

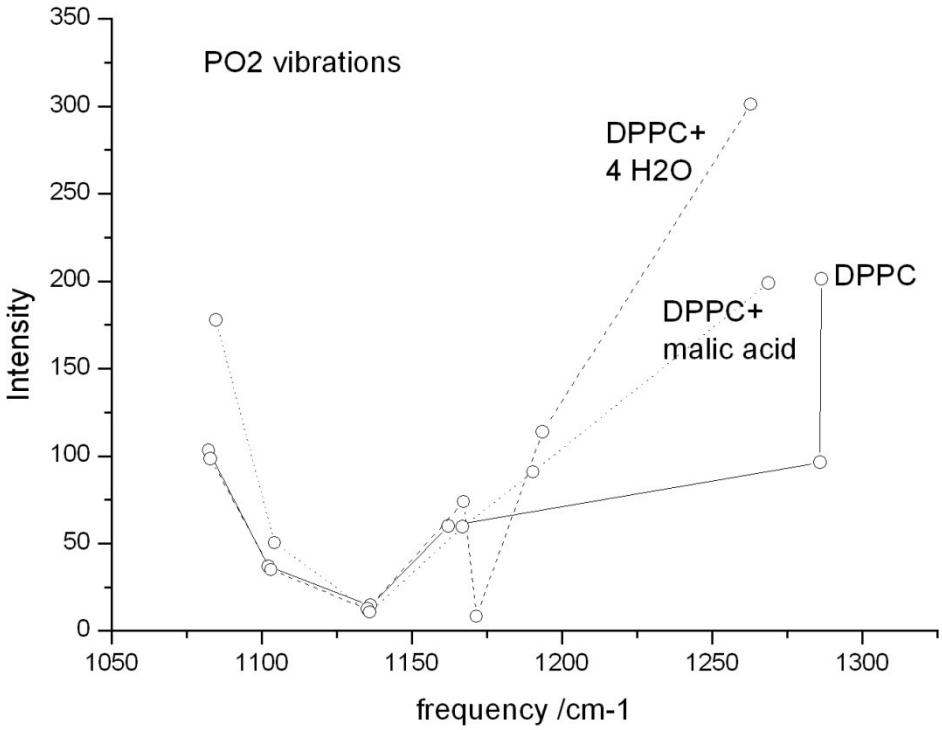

Figure 9. Plot of PO_2^- vibration from a subset of the calculated IR spectrum.

Tables

Table 1. Sample characteristics

Sample name	DPPC/PMLA weight ratio	Medium of hydration
PCPMw01	100:1	Water
PCPMw05	100:5	Water
PCPMb01	100:1	PBS
PCPMb05	100:5	PBS

Table 2. Calorimetric data obtained from DPPC MLVs containing PMLA

Sample name	Pretransition		Main transition	
	T_m (°C)	ΔH (kJ/mol)	T_m (°C)	ΔH (kJ/mol)
DPPC/H_2O	35,7	5,5	41,5	36,6
PCPMw01	33,8	2,3	41,9	34,9
PCPMw05	35,4	1,3	42,0	36,0
DPPC/PBS	35,2	4,4	41,8	34,8
PCPMb01	34,2	3,6	42,1	37,5
PCPMb05	36,2	1,9	41,5	36,5

Table 3. Characteristic distances (d) between layers in MLVs containing PMLA calculated from the first-order peak position (d=1/s) obtained from the SAXS curves

Sample name	$L_{\beta'}$	$P_{\beta'}$	L_{α}
		d (Å)	
DPPC/H_2O	63	71	65
DPPC/PBS	62	71	65
PCPMw01	-	-	-
PCPMw05	-	-	-
PCPMw01 + NaCl	65	67	61
PCPMb01	64	72	68
PCPMb05	68	73	71